J Adv Ceram

Research Article

Low-temperature rapid sintering for the fabrication of biphasic Si_3N_4 ceramics with outstanding mechanical properties

Shuo Zhao[1], Songmo Du[1], Shijia Zhang[1], Dengke Zhao[1], Binbin Fan[1], Bohan Wang[1], Fei Li[1,✉], Kexin Chen[2,✉], Guanghua Liu[1,✉]

Cite this article: Zhao S, Du S, Zhang S, et al. *J Adv Ceram* 2025, **14**(3): 9221044. https://doi.org/10.26599/JAC.2025.9221044

ABSTRACT: The fabrication of Si_3N_4 ceramics typically requires high temperatures (above 1700 °C) and prolonged sintering time to achieve densification, resulting in high energy consumption and increased manufacturing costs. Moreover, reports on the fabrication of dense Si_3N_4 ceramics with good mechanical properties under MPa-level pressure and low temperatures are rare. In this work, we propose a low-temperature rapid spark plasma sintering strategy involving the introduction of fine-grained β-Si_3N_4 powder with high lattice strain energy as an "additive". Dense biphasic Si_3N_4 ceramics, predominantly α-Si_3N_4, were successfully fabricated at a mechanical pressure of 200 MPa and a temperature of 1300 °C, achieving a relative density of 97%. The application of high pressure promoted particle rearrangement and uniform liquid–phase distribution, providing additional driving forces for sintering. The introduction of β-Si_3N_4 seeds facilitated an *in-situ* solution–reprecipitation process, enabling rapid densification with a minimal liquid phase and without significant grain growth, resulting in nanometer-scale grains. The Si_3N_4 sample prepared at 1350 °C exhibited a desirable combination of high hardness (18.5±0.3 GPa) and fracture toughness (6.7±0.2 MPa·m$^{1/2}$). The results demonstrate that by adjusting the sintering temperature and time, the phase composition and mechanical properties of the ceramics can be flexibly tailored. This work holds significant potential for industrial manufacturing and provides valuable insights into low-temperature strategies for ceramic fabrication.

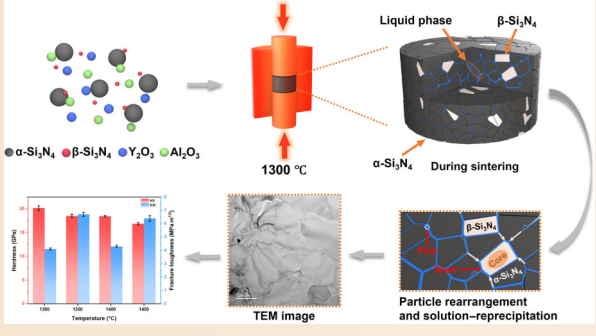

KEYWORDS: low temperature sintering; silicon nitride; β-Si_3N_4 seeds; spark plasma sintering (SPS)

1 Introduction

Silicon nitride ceramics, as high-performance structural-functional integrated ceramics, exhibit high elastic moduli and hardness, excellent high-temperature stability, and good wear resistance. Additionally, they possess chemical stability, such as corrosion resistance, making them indispensable in many critical fields [1–5]. Enhancing the mechanical properties of silicon nitride ceramics has been a goal for researchers [6–8]. However, owing to the strong covalent bonding in silicon nitride, its low self-diffusion coefficient makes densification difficult under solid-phase sintering conditions [9–11]. Therefore, sintering additives are often added during the sintering process to form a liquid phase at high temperatures, thereby achieving densification [12–14]. Although liquid-phase sintering promotes densification, it also facilitates grain growth. It is essential to optimize the sintering process to avoid grain coarsening. Excessive glass phases can reduce the strength of ceramics and impact other properties [15].

The sintering process for silicon nitride typically employs high temperatures and long sintering time to ensure sufficient liquid phase and to promote particle rearrangement and solution–reprecipitation mechanisms for increased density [2,16–18]. However, this inevitably leads to grain coarsening and results in greater energy consumption and time costs. To reduce the sintering temperature and achieve rapid sintering for fine grains, one approach is to use ultrafine silicon nitride powder or special additives such as LiF [19–25], which can achieve densification at relatively low temperatures; however, these methods are characterized by instability and environmental issues [26–28]. Another approach is to increase the sintering pressure, achieving rapid densification at low temperatures and fine grains under pressures close to gigapascal or even several gigapascals [29–31]. However, such high pressures demand stringent requirements for experimental equipment, making it difficult to produce large-sized samples, thus limiting their industrial application [28–30].

Spark plasma sintering (SPS) provides an effective strategy to activate the sintering kinetics of challenging materials, including

[1] State Key Laboratory of New Ceramic Materials, School of Materials Science and Engineering, Tsinghua University, Beijing 100084, China. [2] State Key Laboratory for Advanced Metals and Materials, University of Science and Technology Beijing, Beijing 100083, China.

✉ Corresponding authors. E-mail: F. Li, lif2023@mail.tsinghua.edu.cn; K. Chen, kxchen@ustb.edu.cn; G. Liu, liuguanghua@mail.tsinghua.edu.cn

Received: November 23, 2024; Revised: February 5, 2025; Accepted: February 8, 2025

nanostructured materials, leading to comprehensive improvements in material properties. When SPS is used, hard-to-sinter oxides, nitrides, and carbides are densified by applying a pulsed direct current through a graphite mold, resulting in significant consolidation. Among these materials, Si_3N_4-based ceramics with ultrafine or nanosized grains exhibit tremendous potential for applications in technological and engineering fields [32]. Controlling grain growth during densification is critical for fabricating nanocrystalline ceramics. Compared with conventional sintering methods, SPS enables rapid heating and full densification at lower temperatures and within shorter time. Moreover, as a pressure-assisted pulsed direct current (DC) sintering process, SPS enhances the sintering performance of Si_3N_4, leading to densification with negligible grain growth and phase transformation at low temperatures [33,34]. Additionally, studies have shown that the electric field applied during SPS improves the wettability of the liquid phase, thereby increasing the degree of densification during the initial sintering stages [33].

Typically, the addition of β-Si_3N_4 seeds to silicon nitride ceramics aims to form a self-reinforced microstructure with a bimodal grain size distribution. These seeds act as nucleation sites forβ-phase silicon nitride during sintering, promoting the α-to-β phase transformation and facilitating the development of elongated grains in the final microstructure. This microstructural evolution significantly influences properties such as thermal conductivity, mechanical strength, and tribological performance [35]. In the field of low-temperature sintering, Huang *et al.* [36] demonstrated the use of β-Si_3N_4 seeds (D_{50} ≈ 3 μm, D_{50} means the median diameter), β-Si_3N_4 whiskers (diameter: 1–3 μm, length: 5–20 μm), and TiC particles as additives to coarse industrial Si_3N_4 powders. Hot pressing at 1600 °C under 40 MPa for 30 min produced synergistically reinforced Si_3N_4 ceramic cutting tools with a relative density of 97%, a Vickers hardness of 16.86 GPa, and a fracture toughness of 10.67 MPa·m$^{1/2}$. Xiong *et al.* [37] used rod-like β-Si_3N_4 single-crystal particles (average diameter: 0.53 μm, average length: 4.38 μm) as seeds. Hot pressing at 1700 °C under a mechanical pressure of 30 MPa resulted in dense silicon nitride ceramics with a Vickers hardness of 18.7 GPa and a fracture toughness of 11.2 MPa·m$^{1/2}$. Additionally, Lee *et al.* [38] employed ultrafine β-Si_3N_4 powder (70 nm) as the sole raw material for SPS under a mechanical pressure of 50 MPa. Dense silicon nitride ceramics were achieved at a minimum temperature of 1550 °C, with an average grain diameter of 49.2 nm, a grain length of 101.7 nm, a Vickers hardness of 14 GPa, and a fracture toughness of 3.6 MPa·m$^{1/2}$.

In this work, with conventional Y_2O_3 and Al_2O_3 sintering additives, β-Si_3N_4 seeds were added as another sintering additive. This not only did not reduce sintering activity but also achieved dense silicon nitride ceramics at a minimum temperature of 1300 °C, with a sintering pressure set at 200 MPa. The obtained silicon nitride ceramics exhibited a maximum hardness of 20.2±0.5 GPa and a maximum fracture toughness of 6.7±0.2 MPa·m$^{1/2}$. The effects of β-Si_3N_4 seeds, sintering temperature, and holding time on liquid-phase sintering of silicon nitride were investigated, and the densification mechanism and phase transformation during the sintering process were investigated. Compared with previous studies, this work demonstrated the successful fabrication of dense, large-sized silicon nitride ceramics with excellent mechanical properties at a high heating rate (100 °C/min), short holding time (less than 30 min), and low temperature (1300 °C). This approach significantly reduces production costs, offering considerable value for both engineering applications and academic research.

2 Experimental

2.1 Powder preparations

The initial powders were mixtures of α-Si_3N_4 (SN-E10, oxygen content of 1.27 wt%, UBE Industries Ltd.), Al_2O_3 and Y_2O_3 powders (D_{50} = 0.5 μm, purity > 99.9%, Sinopharm Chemical Reagent Co., Ltd., China), and β-Si_3N_4 (D_{50} = 0.2 μm, Qingdao Alticera Advanced Materials Co., Ltd., China). The starting composition was fixed at a weight ratio of Si_3N_4 : Al_2O_3 : Y_2O_3 = 90 : 6 : 4. The amount of β-Si_3N_4 seeds was 10% by weight with respect to the Si_3N_4 powder. The powders were mixed by wet ball milling for 2 h at 300 r/min with Si_3N_4 balls, and ethanol was used as the mixing medium. Then, the slurry was fully dried and ground through an 80-mesh sieve.

2.2 SPS

Si_3N_4 ceramics were fabricated with liquid phase sintering by SPS. Mixed powders (4 g) were charged into a high-purity graphite die with a diameter of 20 mm surrounded by a porous carbon felt. The samples were sintered using the SPS method (SPS-725, Fuji Electronic Industrial Co., Ltd., Japan) at a heating rate of 100 °C/min. The sintering pressure was set to 200 MPa. The sintering conditions are listed in detail in Table 1.

2.3 Characterizations

An X-ray diffractometer (XRD; D8 Advance, Bruker Co., Germany) with Cu-Kα radiation was used to identify the crystalline phases of the fabricated samples. The morphology of the samples was observed by a field-emission scanning electron

Table 1 Sintering conditions and properties of samples

Sample	Sintering temperature (°C)	Holding time (min)	Relative density (%)	α-Si_3N_4 content (%)	Hardness (GPa)	Fracture toughness (MPa·m$^{1/2}$)
1300-30	1300	30	97	89	20.2±0.5	4.1±0.1
1350-30	1350	30	99	88	18.5±0.3	6.7±0.2
1400-3	1400	3	97	88	18.4±0.2	5.2±0.1
1400-5	1400	5	98	89	18.3±0.3	5.7±0.2
1400-30	1400	30	99	78	18.5±0.2	4.3±0.1
1450-3	1450	3	98	88	18.8±0.2	5.9±0.2
1450-5	1450	5	99	82	18.6±0.3	5.9±0.2
1450-30	1450	30	99	33	16.9±0.2	6.4±0.2
Ref. [39]	—	—	—	99	19.3±0.6	3.2±0.1
Ref. [40]	—	—	—	93	18.0±0.4	4.8±0.4
Ref. [41]	—	—	—	92	17.5±0.1	6.1±0.5
Ref. [42]	—	—	—	0	14.1±0.3	7.0±0.4

microscope (FESEM; Merlin, Zeiss, Germany). No less than 400 grains were selected from the electron microscope images, and their grain size values were measured using Image J. The obtained data were then used to analyze and plot the grain size distribution of the samples. The hardness of the sample was tested with a load of 9.8 N for 15 s by a Vickers hardness tester (TH700, Beijing TIME High Technology Ltd., China). The fracture toughness was estimated by the indentation method with a load of 49 N for 15 s by the Vickers hardness tester [43,44]. Each data point for mechanical properties was measured at least 10 times. The α-Si_3N_4 content mentioned below refers to the weight percentage of α-Si_3N_4 within the total Si_3N_4 phase and was calculated from the XRD data using the method reported by Gazzara and Messier [45]. The density of the sintered samples was determined by the Archimedes method.

3 Results and discussion

3.1 Phase composition

The relative density and α-Si_3N_4 content of the samples are listed in Table 1. The XRD patterns of the initial powders and the samples are shown in Fig. 1. Below 1400 °C, the α-phase content in the silicon nitride ceramic samples is close to 90%, which, compared with the 94% in the initial raw material, indicates that no significant phase transformation has occurred. A content of 94% refers to the content of α-Si_3N_4 in the Si_3N_4 powder, not in the whole powder mixture with sintering aids (Al_2O_3 and Y_2O_3). This value was calculated from the XRD data to maintain consistency with the calculation of α content in the sintered bulk samples. At 1400 °C with holding time of 3 or 5 min, no significant phase transformation occurs. However, when the holding time is extended to 30 min, the α-phase in the samples clearly decreases to 78%, indicating significant α–β phase transformation. This suggests that at lower temperatures, only a small amount of high-viscosity liquid phase is formed, and the viscosity of the liquid is high; accordingly, the phase transformation via the dissolution-reprecipitation process is limited [46,47].

3.2 Sample density

Figure 2 shows the displacement of the lower punch during the holding stage of SPS process, which can be used as a reference for the shrinkage of samples. All four samples undergo rapid shrinkage within the first 5 min, followed by a decrease in the shrinkage speed and complete densification at different time. The lower the sintering temperature, the longer the time required for the samples to achieve densification. At higher sintering temperatures, the samples exhibit greater shrinkage before entering the holding stage, achieving densification earlier, and thus exhibit less shrinkage during the holding stage. During the sintering process of Si_3N_4 ceramics, rapid shrinkage is observed when the temperature exceeds 1350 °C. At a sintering temperature of 1450 °C, substantial densification is achieved prior to the holding stage. Consequently, the additional shrinkage during the holding stage is significantly reduced compared to that of the other three samples sintered at lower temperatures. Additionally, the samples sintered at 1400 and 1450 °C slightly reverse the movement of the lower punch position after rapid densification, possibly related to the thermal expansion of the graphite die [48].

The sample sintered at 1300 °C achieves a relative density of 97%. After holding for 30 min, the lower punch still tends to shrink further, indicating that the densification process is still going on. At higher sintering temperatures, the samples no longer shrink, indicating that the maximum density achievable under these conditions has been reached.

An analysis of samples under different sintering conditions reveals that sintering temperature has a significant effect on the sintering process of silicon nitride ceramics [49,50]. Within this temperature range, an increase of 50 °C can substantially increase the liquid phase content in the system, thereby promoting the densification process. Increasing the sintering temperature can significantly reduce the time required for densification. However, holding at 1300 °C for 30 min can also achieve a relative density of 97%, which essentially indicates that densification has been achieved for ceramics.

3.3 Microstructures of raw powders and sintered samples

Figure 3 displays the microstructures of all 8 samples. Figure 3 shows that most of the four samples consist of equiaxed α-Si_3N_4 grains, with only a small portion of rod-like β-Si_3N_4 grains. The grain size ranges from 100 to 200 nm, with only a few grains exceeding 500 nm in size. The reasons why dense silicon nitride ceramics can be obtained at lower sintering temperatures of 1300–1400 °C than traditional sintering methods (e.g., 1700–1900 °C) are discussed below.

A schematic diagram of densification mechanism of Si_3N_4 ceramics is shown in Fig. 4. From the perspective of high sintering pressure, on one hand, high pressure can crush agglomerates in the green body, making the pore sizes in the raw powders smaller than the grain sizes, increasing the dihedral angle and raising the critical coordination number of pores. Consequently, the number of grains surrounding the pores decreases than the critical coordination number, leading to shrinkage of pores [51]. On the other hand, high pressure can provide an additional driving force

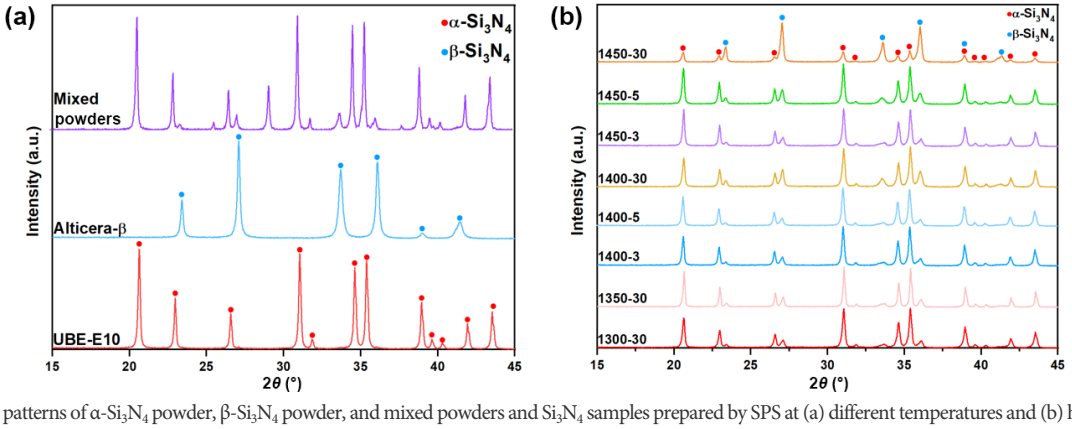

Fig. 1 XRD patterns of α-Si_3N_4 powder, β-Si_3N_4 powder, and mixed powders and Si_3N_4 samples prepared by SPS at (a) different temperatures and (b) holding time.

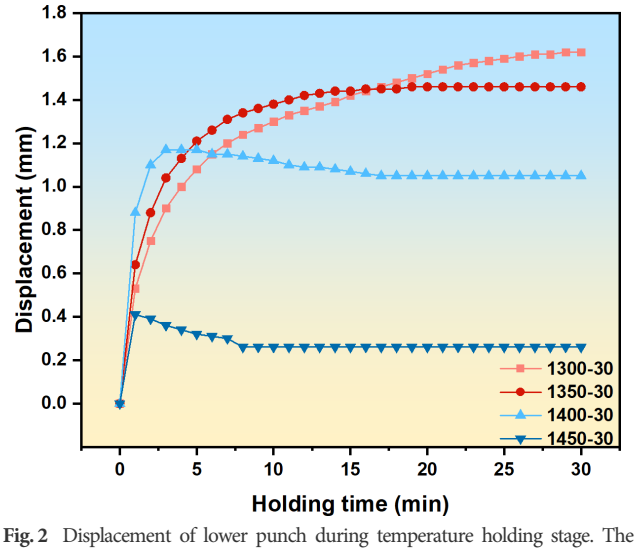

Fig. 2 Displacement of lower punch during temperature holding stage. The displacement was normalized to zero at the beginning of holding stage.

for sintering, accelerating the densification rate. In addition to the capillary force of the liquid phase, high sintering pressure provides additional mechanical pressure, further promoting particle rearrangement [39]. From the perspective of low sintering temperature, lower temperatures can reduce grain growth, leading to an increased specific surface area and reduced intergranular distances. These factors enhance diffusion kinetics by shortening the diffusion distance [52].

During the liquid-phase sintering of silicon nitride, low-temperature sintering produces less liquid phase than traditional sintering methods. According to Table 1, the final α-phase content in samples 1300-30 and 1350-30 is slightly less than 94%, indicating that there is no significant phase transformation. However, significant phase transformation occurred in samples 1400-30 and 1450-30, with the α-phase content substantially decreasing. This suggests that the solution–reprecipitation mechanism plays an important role in densification during low-temperature SPS sintering with β-Si_3N_4 seeds. Thus, the densification mechanism of low-temperature sintered samples can be attributed to the coupled interaction of particle rearrangement and solution–reprecipitation. First, a high sintering pressure promotes particle rearrangement and facilitates the uniform distribution of the liquid phase within the body [53], which in turn promotes the solution–reprecipitation process. The introduction of fine-grained β-Si_3N_4 seeds with higher lattice strain energy promotes the solution–reprecipitation process to a certain extent. The solution–reprecipitation process can then fill the remaining small pores after particle rearrangement, further enhancing the densification of samples.

This is also evidenced in the transmission electron microscopy (TEM) images shown in Fig. 5, where a distinct core–shell structure can be observed. This indicates that new β-Si_3N_4 has precipitated on the surface of the seeds through solution and reprecipitation [35]. This suggests that solution–reprecipitation can significantly increase the degree of densification during low-temperature sintering.

3.4 XRD data fitting

Figure 1 shows that the full width at half maximum (FWHM) of the β-Si_3N_4 powder is significantly greater than that of the α-Si_3N_4 powder. This broadening may be caused by grain refinement and lattice strain [54], as expressed in Eqs. (1) and (2), where β is the FWHM; k is a constant, which is taken as 1 here; λ is the X-ray wavelength; D is the grain size; θ is the diffraction angle; ε is the lattice strain. The contributions of grain refinement and lattice strain to the broadening effect can be estimated by fitting according to Eq. (3). By this method (Fig. 6), the lattice strain (ε) is 1.2×10^{-3}, and the average grain size (D) is approximately 90 nm. The presence of nanoparticles and lattice strain in the β-Si_3N_4 powder may promote sintering. The mechanism can be attributed primarily to the following two factors: (1) Particle size effect. Ultrafine particles possess a large specific surface area and reduced interparticle distances, which enhance the atomic diffusion efficiency during the sintering process. Compared with larger particles, ultrafine particles can initiate sintering at lower temperatures, forming strong bonds. These particles exhibit higher surface energy and smaller grain sizes, reducing the required sintering time and temperature, thereby enabling low-temperature sintering. (2) Contribution of high lattice strain energy. A high lattice strain energy corresponds to a high density of structural defects. From a thermodynamic perspective, higher energy correlates with higher sintering activity, thereby promoting the sintering process. From a kinetic perspective, a higher density of structural defects provides additional rapid diffusion pathways, enhancing diffusion and accelerating mass transfer. Therefore, the addition of β-Si_3N_4 particles with high lattice strain energy can effectively reduce the critical sintering temperature and promote densification at lower temperatures.

$$\beta = \frac{k \cdot \lambda}{D \cdot \cos\theta} \tag{1}$$

$$\beta = 4\varepsilon \cdot \tan\theta \tag{2}$$

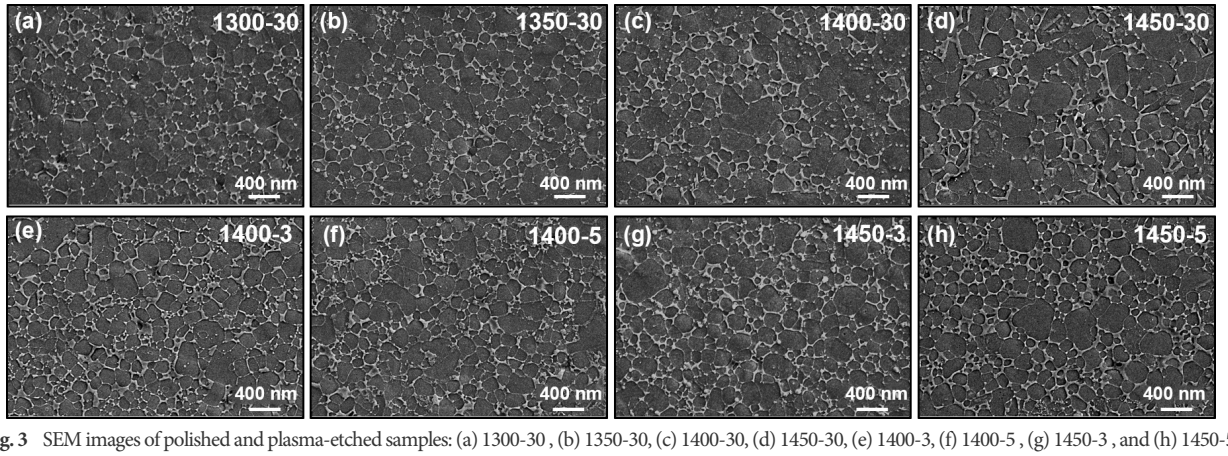

Fig. 3 SEM images of polished and plasma-etched samples: (a) 1300-30 , (b) 1350-30, (c) 1400-30, (d) 1450-30, (e) 1400-3, (f) 1400-5 , (g) 1450-3 , and (h) 1450-5.

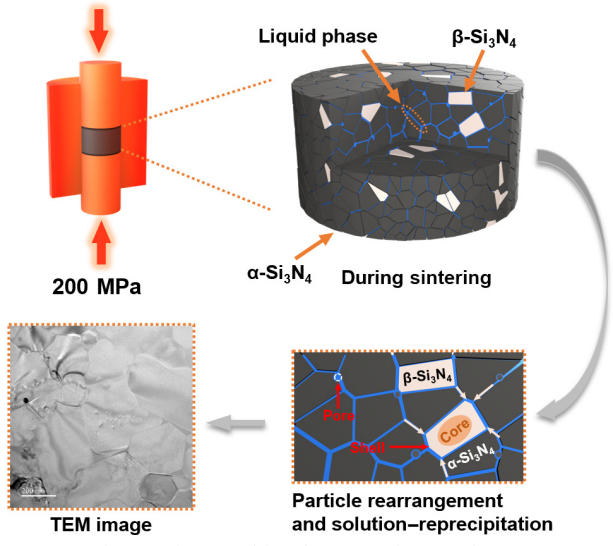

Fig. 4 Schematic diagram of densification mechanism of Si_3N_4 ceramics.

$$\frac{\beta\cos\theta}{\lambda} = \frac{1}{D} + 4\varepsilon\frac{\sin\theta}{\lambda} \quad (3)$$

Figure 7 shows the morphology ofα-Si_3N_4 powder and β-Si_3N_4 seeds added to the raw material. Moreover, as shown in Fig. 7, α-Si_3N_4 powder and β-Si_3N_4 seeds consist of particles with an average size of 200 nm and some smaller nanoparticles (50 nm). No nanoparticles were found in the sintered samples, indicating that the introduction of seeds promoted the dissolution of these particles in the liquid phase. The relatively large β-Si_3N_4 particles can act as seeds, promoting phase transformation to some extent. These combined factors enable the achievement of dense silicon nitride ceramics at a low temperature of 1300 °C.

3.5 Particle size distributions of samples

The particle size distributions of the samples are shown in Fig. 8. The average grain size (G_{avg}) of the samples is labeled in Fig. 8. The Hillert σ, which is the ratio of the standard deviation (Σ) of the grain-size distribution to the average grain size (G_{avg}) of the samples [55], is in the range of 0.38–0.51. As the sintering temperature increases, the percentage of grains with a size less than 100 nm gradually decreases, which is consistent with the well-known effect of higher sintering temperatures promoting grain coarsening. The grain sizes of all samples are less than 200 nm. The sample 1300-30 has the smallest average grain size of 147 nm, followed by 1450-3, with an average grain size of 156 nm, which is likely due to its shorter holding time. This indicates that to achieve grain refinement, it is essential to lower the sintering temperature and shorten the holding time. Since the activation energy for densification is generally greater than that for grain coarsening, the high pressure and rapid heating characteristics of SPS can enable the densification rate to surpass the grain coarsening rate, thus achieving rapid densification without significant grain growth.

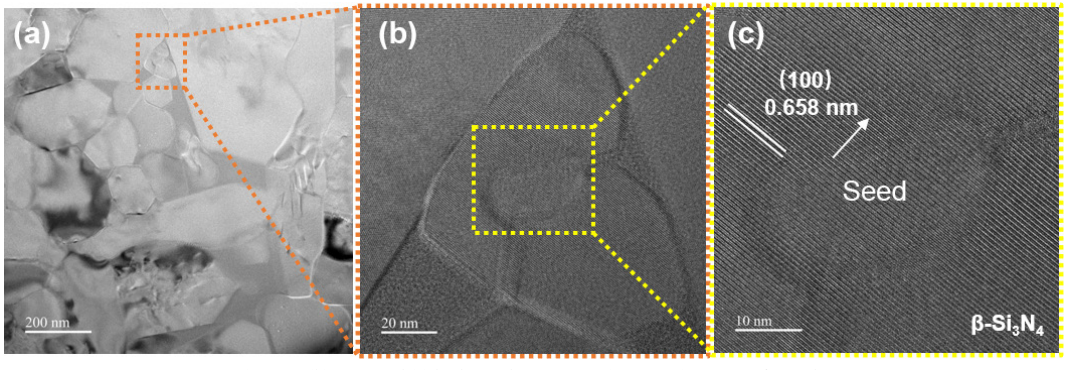

Fig. 5 (a) TEM, (b) BFI , and (c) high-resolution TEM (HRTEM) images of sample 1450-30.

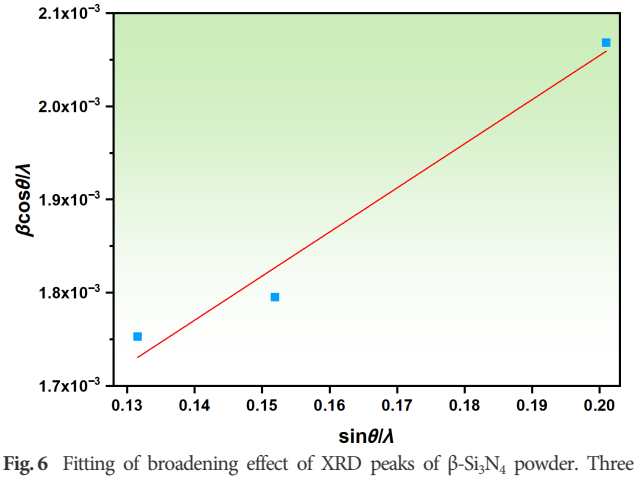

Fig. 6 Fitting of broadening effect of XRD peaks of β-Si_3N_4 powder. Three strong peaks, (110), (200), and (210), are used, and instrument broadening is subtracted.

3.6 Mechanical properties

The mechanical properties of the samples obtained at different sintering temperatures and holding time are shown in Fig. 9. A comparison with other studies is shown in Table 1. The hardness values of the samples held for 30 min at different temperatures are above 16.9 GPa, with the highest value reaching 20.2±0.5 GPa. The fracture toughness values are all above 4.1 MPa·$m^{1/2}$, with the highest value reaching 6.7±0.2 MPa·$m^{1/2}$. The hardness values of the samples obtained at 1450 °C with different holding time are all above 16.9 GPa, with the highest reaching 18.8±0.2 GPa; the fracture toughness values are all above 5.9 MPa·$m^{1/2}$, with the highest reaching 6.4±0.2 MPa·$m^{1/2}$.

Among all the samples, 1300-30 has the highest hardness values. Generally, the hardness is influenced by multiple factors, including relative density, phase composition, and grain size. The higher hardness of sample 1300-30 should be attributed to its higher α-Si_3N_4 content (Table 1) and smaller grain size (Fig. 8). Although the relative density of the sample 1300-30 (97%) is slightly lower than those of other samples (98%–99%), it is sufficient to ensure that most open pores have been removed and

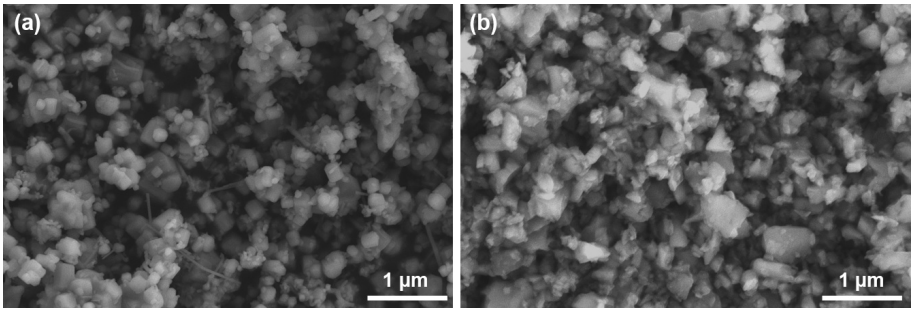

Fig. 7 SEM images of (a) raw α-Si_3N_4 powder and (b) β-Si_3N_4 powder.

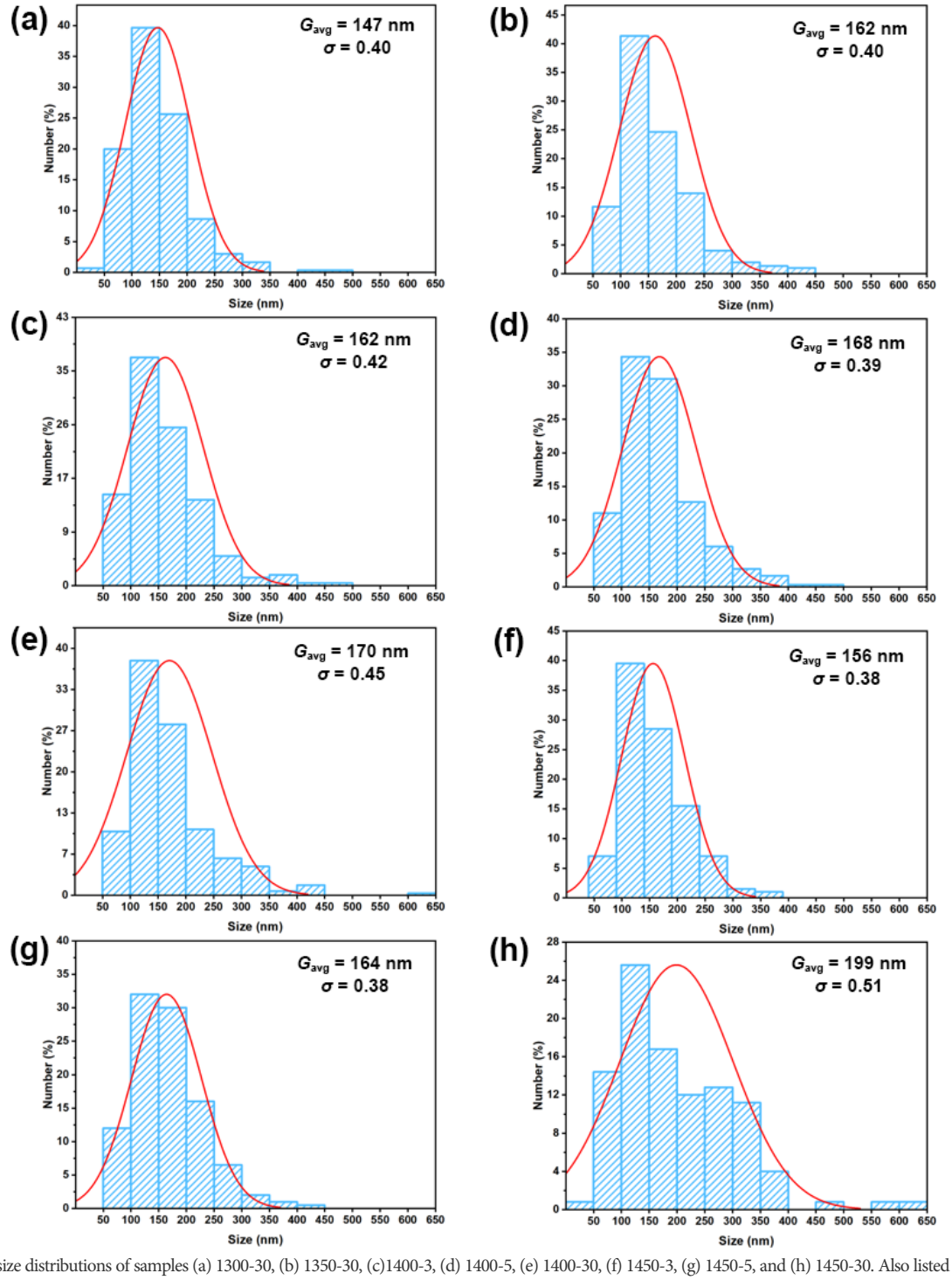

Fig. 8 Grain size distributions of samples (a) 1300-30, (b) 1350-30, (c)1400-3, (d) 1400-5, (e) 1400-30, (f) 1450-3, (g) 1450-5, and (h) 1450-30. Also listed in histograms are G_{avg} and σ.

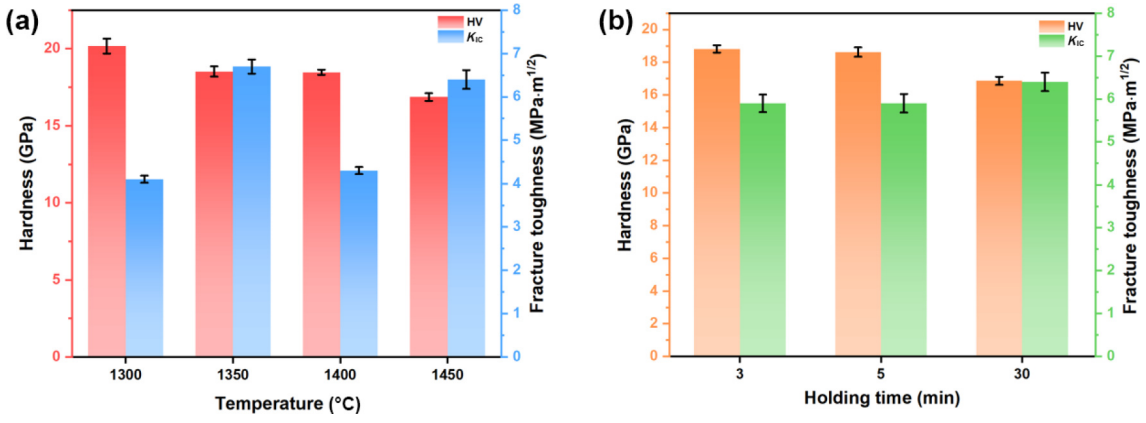

Fig. 9 Mechanical properties of (a) samples at different temperatures for 30 min and (b) samples at different holding time at 1450 °C .

the remaining pores are predominantly isolated closed pores, which is unlikely to cause a significant decrease in hardness.

Among all the samples, samples 1350-30 exhibit the highest fracture toughness values. The SEM images of the indentations and cracks are shown in Fig. 10. The SEM images reveal that although most samples predominantly consist of equiaxed grains without the formation of many elongated β-Si_3N_4 grains, the primary crack propagation mode is intergranular fracture. This highly tortuous path significantly dissipates the energy associated with crack propagation. Moreover, frequent crack bifurcations are evident around the grain boundaries in sample 1350-30 (as shown in Fig. 10), which further enhances the fracture toughness.

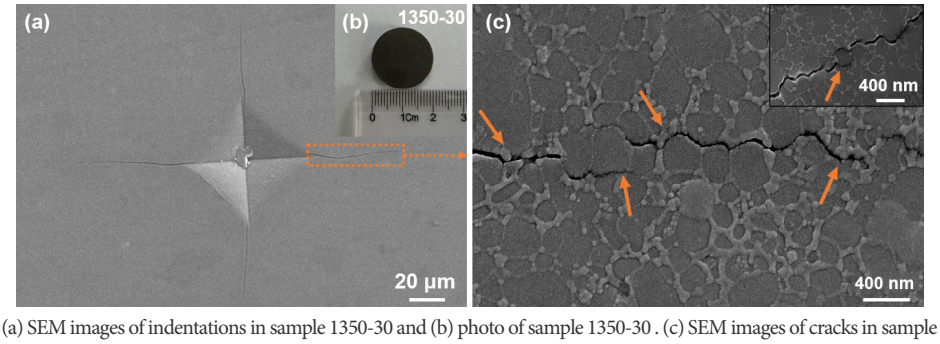

Fig. 10 (a) SEM images of indentations in sample 1350-30 and (b) photo of sample 1350-30 . (c) SEM images of cracks in sample 1350-30.

4 Conclusions

Commercial α-Si_3N_4 was used as the raw material, and β-Si_3N_4 seeds were added as sintering additives on the basis of conventional Y_2O_3 and Al_2O_3 sintering additives. Dense silicon nitride ceramics with a relative density of 97% and α-Si_3N_4 content of 89% were obtained through SPS at a minimum temperature of 1300 °C. This approach employs high pressure to promote particle rearrangement and introduces ultrafine β-Si_3N_4 seeds to facilitate solution–reprecipitation, resulting in the fabrication of dense fine-grained silicon nitride ceramics. During the low-temperature sintering of silicon nitride, the coupled interaction of particle rearrangement and solution–reprecipitation effectively increases the degree of densification. The average grain size is approximately 150 nm, with sample 1350-30 achieving a hardness of 18.5±0.3 GPa and a fracture toughness of 6.7±0.2 MPa·m$^{1/2}$. This makes the rapid low-temperature preparation of dense silicon nitride ceramics with controllable phase composition possible.

Acknowledgements

This work was supported by the National Natural Science Foundation of China (Nos. 52425204, U20A20241, and U23A20566).

Declaration of competing interest

The authors have no competing interests to declare that are relevant to the content of this article.

References

[1] Riley FL. Silicon nitride and related materials. *J Am Ceram Soc* 2000, **83**: 245–265.
[2] Petzow G, Herrmann M. Silicon nitride ceramics. In: *High Performance Non-Oxide Ceramics II*. Berlin (Germany): Springer, 2002: 47–167.
[3] Zhang J, Liu GH, Cui W, *et al.* Plastic deformation in silicon nitride ceramics via bond switching at coherent interfaces. *Science* 2022, **378**: 371–376.
[4] Krstic Z, Krstic VD. Silicon nitride: The engineering material of the future. *J Mater Sci* 2012, **47**: 535–552.
[5] Xue WJ, Yi J, Xie ZP, *et al.* Enhanced fracture toughness of silicon nitride ceramics at cryogenic temperatures. *Scripta Mater* 2012, **66**: 891–894.
[6] Du XY, Lee SS, Blugan G, *et al.* Silicon nitride as a biomedical material: An overview. *Int J Mol Sci* 2022, **23**: 6551.
[7] Kondo N, Asayama M, Suzuki Y, *et al.* High-temperature strength of sinter-forged silicon nitride with Lutetia additive. *J Am Ceram Soc* 2003, **86**: 1430–1432.
[8] Zhao S, Du SM, Sun SY, *et al.* Synthesis of spherical Si_3N_4 powders by liquid-phase modified carbothermal reduction and nitridation. *J Am Ceram Soc* 2024, **107**: 16–23.
[9] Han Y, Xie ZP, Li S, *et al.* Optimum sintering temperature of high quality silicon nitride ceramics under oscillatory pressure. *Ceram Int* 2018, **44**: 6949–6952.
[10] Yang JF, Ohji T, Niihara K. Influence of yttria–alumina content on sintering behavior and microstructure of silicon nitride ceramics. *J Am Ceram Soc* 2000, **83**: 2094–2096.
[11] Kingery WD. Densification during sintering in the presence of a liquid phase. I. Theory. *J Appl Phys* 1959, **30**: 301–306.

[12] German RM. *Liquid Phase Sintering*. New York (USA): Plenum Press, 1985.
[13] German RM. *Sintering Theory And Practice*. New York (USA): Wiley, 1996.
[14] Sharma V, Nemat-Nasser S, Vecchio KS. Effect of grain-boundary phase on dynamic compression fatigue in hot-pressed silicon nitride. *J Am Ceram Soc* 1998, **81**: 129–139.
[15] Ziegler G, Heinrich J, Wötting G. Relationships between processing, microstructure and properties of dense and reaction-bonded silicon nitride. *J Mater Sci* 1987, **22**: 3041–3086.
[16] Du SM, Zhang J, Li F, *et al.* Rapid fabrication of Si_3N_4 ceramics with gradient appearance and microstructure. *J Am Ceram Soc* 2023, **106**: 7611–7617.
[17] Imamura H, Kawata T, Honda S, *et al.* Thermal conductivity improvement in silicon nitride ceramics via grain purification. *J Am Ceram Soc* 2024, **107**: 1159–1169.
[18] Zhang J, Cui W, Li F, *et al.* Effects of $MgSiN_2$ addition and post-annealing on mechanical and thermal properties of Si_3N_4 ceramics. *Ceram Int* 2020, **46**: 15719–15722.
[19] Xu X, Nishimura T, Hirosaki N, *et al.* Fabrication of a nano-Si_3N_4/nano-C composite by high-energy ball milling and spark plasma sintering. *J Am Ceram Soc* 2007, **90**: 1058–1062.
[20] Bake A, Hakeem AS, Ahmed BA, *et al.* Effect of nano- and micro-sized Si_3N_4 powder on phase formation, microstructure and properties of β′ -SiAlON prepared by spark plasma sintering. *Ceram Int* 2022, **48**: 1916–1925.
[21] Yang M, Wang Q, Lv ML, *et al.* Synthesis and sintering of silicon nitride nano-powders via sodium reduction in liquid ammonia. *J Eur Ceram Soc* 2016, **36**: 1899–1904.
[22] Xu X, Nishimura T, Hirosaki N, *et al.* New strategies for preparing nanosized silicon nitride ceramics. *J Am Ceram Soc* 2005, **88**: 934–937.
[23] Matovic B, Rixecker G, Aldinger F. Densification of Si_3N_4 with $LiYO_2$ additive. *J Am Ceram Soc* 2004, **87**: 546–549.
[24] Luo J, Li JG, Li MJ, *et al.* Low-temperature densification by plasma activated sintering of Mg_2Si-added Si_3N_4. *Ceram Int* 2019, **45**: 15128–15133.
[25] Luo CX, Zhang YX, Deng TF. Pressureless sintering of high performance silicon nitride ceramics at 1620 °C. *Ceram Int* 2021, **47**: 29371–29378.
[26] Yang HB, Wang BM, Zhang H, *et al.* Evolving corundum nanoparticles at room temperature. *Acta Mater* 2023, **255**: 119038.
[27] Wen QB, Yu ZJ, Riedel R. The fate and role of *in situ* formed carbon in polymer-derived ceramics. *Prog Mater Sci* 2020, **109**: 100623.
[28] Johnston NR, Strobel SA. Principles of fluoride toxicity and the cellular response: A review. *Arch Toxicol* 2020, **94**: 1051–1069.
[29] Gasch MJ, Wan J, Mukherjee AK. Preparation of a Si_3N_4/SiC nanocomposite by high-pressure sintering of polymer precursor derived powders. *Scripta Mater* 2001, **45**: 1063–1068.
[30] Jia HS, Li JQ, Niu R, *et al.* Fabrication of β-Si_3N_4 with high thermal conductivity under ultra-high pressure. *Ceram Int* 2018, **44**: 23288–23292.
[31] Ma SL, Zhao YS, Tang RL, *et al.* Transparent β-Si_3N_4 and γ-Si_3N_4 compacts synthesized with mixed-size precursor under high pressure and high temperature. *Appl Phys Lett* 2021, **119**: 171904.
[32] Ratzker B, Sokol M. Exploring the capabilities of high-pressure spark plasma sintering (HPSPS): A review of materials processing and properties. *Mater Des* 2023, **233**: 112238.
[33] Miranzo P, González-Julián J, Osendi MI, *et al.* Enhanced particle rearrangement during liquid phase spark plasma sintering of silicon nitride-based ceramics. *Ceram Int* 2011, **37**: 159–166.
[34] Jeong K, Tatami J, Iijima M, *et al.* Spark plasma sintering of silicon nitride using nanocomposite particles. *Adv Powder Technol* 2017, **28**: 37–42.
[35] Govindasamy L, Park YJ, Ko JW, *et al.* Role of β-Si_3N_4 seeds in microstructure development and properties of silicon nitride ceramics: A comprehensive review. *J Korean Ceram Soc* 2024, **61**: 507–536.
[36] Huang JW, Lv XA, Dong XF, *et al.* Synergistic reinforcement of Si_3N_4 based ceramics fabricated via multiphase strengthening under low temperature and short holding time. *Materials* 2023, **16**: 6163.
[37] Xiong H, Li B, Xi XA, *et al.* Preparation of graded silicon nitride ceramics with high mechanical performance using β-Si_3N_4 seeds. *Ceram Int* 2023, **49**: 36528–36535.
[38] Lee CH, Lu HH, Wang CG, *et al.* Microstructure and fracture behavior of β-Si_3N_4 based nanoceramics. *Ceram Int* 2011, **37**: 641–645.
[39] Du SM, Zhang J, Li F, *et al.* Low temperature fabrication of highly dense α-Si_3N_4 ceramics. *J Am Ceram Soc* 2024, **107**: 4494–4500.
[40] Wang B, Jiang QG, Liu WY, *et al.* Fabrication of fine-grained α/β Si_3N_4 by hot pressing flowing sintering at 1550 °C. *Ceram Int* 2019, **45**: 13958–13963.
[41] Ratzker B, Sokol M, Kalabukhov S, *et al.* High-pressure spark plasma sintering of silicon nitride with LiF additive. *J Eur Ceram Soc* 2018, **38**: 1271–1277.
[42] Kumar K, Kim MJ, Oh HM, *et al.* Fabrication of highly dense Si_3N_4 via record low-content additive system for low-temperature pressureless sintering. *J Am Ceram Soc* 2022, **105**: 4669–4680.
[43] Niihara K. A fracture mechanics analysis of indentation-induced Palmqvist crack in ceramics. *J Mater Sci Lett* 1983, **2**: 221–223.
[44] Niihara K, Morena R, Hasselman DPH. Evaluation of K_{IC} of brittle solids by the indentation method with low crack-to-indent ratios. *J Mater Sci Lett* 1982, **1**: 13–16.
[45] Gazzara C, Messier D. Determination of phase content of Si_3N_4 by X-ray diffraction analysis. *Am Ceram Soc Bull* 1977, **56**: 777–780.
[46] Hampshire S, Nestor E, Flynn R, *et al.* Yttrium oxynitride glasses: Properties and potential for crystallisation to glass-ceramics. *J Eur Ceram Soc* 1994, **14**: 261–273.
[47] Saito N, Kai K, Furusho S, *et al.* Properties of nitrogen-containing yttria–alumina–silica melts and glasses. *J Am Ceram Soc* 2003, **86**: 711–716.
[48] Sayyadi-Shahraki A, Rafiaei SM, Ghadami S, *et al.* Densification and mechanical properties of spark plasma sintered Si_3N_4/ZrO_2 nano-composites. *J Alloys Compd* 2019, **776**: 798–806.
[49] Kang SL, Jung YI. Sintering kinetics at final stage sintering: Model calculation and map construction. *Acta Mater* 2004, **52**: 4573–4578.
[50] Kang SJL. *Sintering*. Oxford (UK): Elsevier, 2005.
[51] Delannay F. The role of dihedral angle on the control of skeleton coordination and pore closure in aggregates driven by capillary forces. *Scripta Mater* 2010, **62**: 928–933.
[52] Kocjan A, Logar M, Shen ZJ. The agglomeration, coalescence and sliding of nanoparticles, leading to the rapid sintering of zirconia nanoceramics. *Sci Rep* 2017, **7**: 2541.
[53] Liu Y, Wu H, Chen GH. Enhanced mechanical properties of nanocomposites at low graphene content based on *in situ* ball milling. *Polym Compos* 2016, **37**: 1190–1197.
[54] Jiang CH, Yang CZ. *X-ray Diffraction Technology and Its Application*. Shanghai (China): East China University of Science and Technology Press, 2010. (in Chinese)
[55] Dong YH, Yang HB, Zhang L, *et al.* Ultra-uniform nanocrystalline materials via two-step sintering. *Adv Funct Mater* 2021, **31**: 2007750.